Phonon spectrum of $Pr_2Zr_2O_7$ and $Pr_2Ir_2O_7$ as evidence of coupling of the lattice with electronic and magnetic degrees of freedom

Yuanyuan Xu [1], Huiyuan Man,[1,2] Nan Tang [2], Takumi Ohtsuki,[2] Santu Baidya,[3] Satoru Nakatsuji,[1,2,4,5,6] David Vanderbilt [3], and Natalia Drichko[1]

[1]*Institute for Quantum Matter and Department of Physics and Astronomy, Johns Hopkins University, Baltimore, Maryland 21218, USA*
[2]*Institute for Solid State Physics, University of Tokyo, Kashiwa, Chiba 277-8581, Japan*
[3]*Department of Physics and Astronomy, Rutgers University, Piscataway, New Jersey 08854-8019, USA*
[4]*Department of Physics, University of Tokyo, Bunkyo-ku, Tokyo 113-0033, Japan*
[5]*CREST, Japan Science and Technology Agency, Kawaguchi, Saitama 332-0012, Japan*
[6]*Trans-scale Quantum Science Institute, University of Tokyo, Bunkyo-ku, Tokyo 113-0033, Japan*

Magnetic materials with pyrochlore crystal structure form exotic magnetic states due to the high lattice frustration. In this work we follow the effects of coupling of the lattice and electronic and magnetic degrees of freedom in two praseodymium-based pyrochlores $Pr_2Zr_2O_7$ and $Pr_2Ir_2O_7$. In either of these materials, the presence of magnetic interactions does not lead to magnetically ordered low temperature states; however, their electronic properties are different. A comparison of Raman phonon spectra of $Pr_2Zr_2O_7$ and $Pr_2Ir_2O_7$ allows us to identify magnetoelastic coupling in $Pr_2Zr_2O_7$ that elucidates its magnetic properties at intermediate temperatures and allows us to characterize phonon-electron scattering in the semimetallic $Pr_2Ir_2O_7$. We also show that the effects of random disorder on the Raman phonon spectra is small.

I. INTRODUCTION

Frustrated magnetism and the search for spin liquid materials is one of the main topics of condensed matter physics in recent years. The pyrochlore crystal structure provides a geometrically frustrated lattice suitable for hosting classical and quantum spin-ice and spin liquid states [1–3].

In this work we present a phonon Raman scattering study of praseodymium-based pyrochlores $Pr_2Zr_2O_7$ and $Pr_2Ir_2O_7$. These compounds have very similar crystal structures [4,5], and in both materials Pr^{3+} is in the magnetic $J = 4$ state. Despite the presence of magnetic interactions, the highest quality samples do not order magnetically down to the lowest measured temperatures for either of these compounds. These two materials are rarely discussed together due to the drastically different electronic properties. We found that a comparative study of their phonon spectra can reveal valuable information about the coupling of the lattice to magnetic and electronic degrees of freedom which is difficult to identify otherwise.

In the electronic structure of $Pr_2Ir_2O_7$ the bands around the Fermi surface are formed by Ir^{4+} orbitals. Due to the spin-orbit coupling, the bands split so that the resulting magnetic moment of Ir^{4+} is $J_{eff} = 1/2$ [6]. This material is suggested to be a Luttinger semimetal, that is to host a quadratic band touching at the Γ point of the Brillouin zone (BZ) [4]. Resistivity in $Pr_2Ir_2O_7$ decreases on cooling and flattens below 50 K due to a Kondo effect [7]. Due to the presence of the itenerant charge carriers, magnetic interactions are predominantly of Ruderman-Kittel-Kasuya-Yosida type. Early on it was suggested to be a chiral metallic spin liquid [7–10].

Due to a closed shell of Zr^{4+} with $J = 0$, $Pr_2Zr_2O_7$ is an insulator with a band gap of about 3.5 eV [see the band structure calculations presented in the Supplemental Material (SM), Fig. S4 [11]]. Magnetic interactions are Ising-like as typical for rare earth [2], and thus the material is a quantum spin ice candidate [12].

While these two compounds are relatively well studied, the origin of their low temperature states is still under discussion. In both of these materials, structural disorder was claimed to influence the low temperature state [12–15], but other subtle effects related to the magnetoelastic interactions and phonon-electron scattering for metallic $Pr_2Ir_2O_7$ can be important.

In this work, we use phonon Raman spectroscopy, together with density functional theory (DFT) calculations, to study $Pr_2Zr_2O_7$ and $Pr_2Ir_2O_7$. Raman scattering has shown its high sensitivity to magnetoelastic coupling, small lattice distortions, and structural disorder [16]. Somewhat unexpectedly, we do not find any significant effects of random disorder on the Raman spectra of these materials. For both of them the only phonons that show broadening and splitting are E_g phonons, which can be associated with the tilting of octahedra as discussed in Ref. [17]. A very similar phonon spectrum originated from the similar crystal structures but different electronic properties allow us to identify phonon-electron scattering in $Pr_2Ir_2O_7$ and effects of magnetoelastic coupling in $Pr_2Zr_2O_7$.

TABLE I. Components of Raman tensor for (x, x) and (x, y) polarizations.

Geometry	A_{1g}	E_g	T_{2g}
(x, x)	a^2	b^2	c^2
(x, y)	0	b^2	$\frac{2}{3}c^2$

II. METHODS

Polarized Raman scattering spectra were measured from (111) surface of the $Pr_2Zr_2O_7$ and $Pr_2Ir_2O_7$ single crystals grown by the floating zone method and the flux method, respectively [4,18]. Raman scattering was excited with 514.5 nm and 647 nm lines of Ar^+-Kr^+ mixed gas laser. Raman spectra were measured using the Jobin-Yvon T64000 triple monochromator spectrometer with a liquid nitrogen cooled CCD detector in the temperature range from 300 down to 14 K and in the frequency range from 800 down to about $30\,cm^{-1}$.

The pyrochlore lattice has $Fd\bar{3}m$ (No. 227) space group corresponding to O_h point group. The polarization-resolved spectra were measured in (x, x) and (x, y) geometries, where x denotes an arbitrary direction in the (111) plane and y is perpendicular to x. In Table I we present what symmetries of scattering channels are observed in the two measured geometries.

We used the plane-wave pseudopotential method as implemented in the Vienna *ab initio* simulation package (VASP) for the calculation of the electronic band structure and phonon frequencies of $Pr_2Zr_2O_7$ and $Pr_2Ir_2O_7$ [19]. The calculation was done for the nonmagnetic configuration with Pr f electrons in the core. The calculations were carried out using a generalized gradient approximation (PBE-GGA) [20–22] to the exchange-correlation potential, a $4 \times 4 \times 4$ k-point grid, and a plane-wave cutoff energy of 500 eV. Spin-orbit coupling was included as implemented in VASP.

III. RESULTS

Raman scattering spectra of the single crystals of $Pr_2Zr_2O_7$ and $Pr_2Ir_2O_7$ in the spectral range between 150 and 800 cm^{-1} in (x, x) scattering channel at $T = 14$ K are presented in Fig. 1, while temperature dependence of the spectra is shown in Fig. 2 for $Pr_2Zr_2O_7$ and Fig. 3 for $Pr_2Ir_2O_7$. The low temperature data allows one to resolve not only phonon excitations, but also crystal electric field (CEF) excitations [23]. This spectral range covers all Raman-active phonons and CEF excitations except the lowest CEF excited state at about 80 cm^{-1} discussed in Ref. [23]. Due to the similarities of the crystal structure, many of the observed excitations show similar energies in these two compounds; however, the Raman response of $Pr_2Ir_2O_7$ is approximately two orders of magnitude weaker than that of $Pr_2Zr_2O_7$, due to the fact that the first material is metallic and screening reduces the Raman response.

Raman-active phonons marked by red color in Fig. 1 are discussed in details in this work. CEF excitations of Pr^{3+} (marked by green in Fig. 1) were assigned based on the neutron scattering results for these two materials [24–26]. Raman

FIG. 1. Raman scattering spectra of (a) $Pr_2Ir_2O_7$ and (b) $Pr_2Zr_2O_7$ at 14 K in parallel polarization configuration. Solid black curve shows the experimental data after a linear background subtraction. Dashed gray line shows the overall fitting.

scattering on CEF excitations in $Pr_2Zr_2O_7$ is discussed in Ref. [23]. In $Pr_2Ir_2O_7$ spectra, we observe distinctly only the CEF excitation at around 460 cm^{-1}. The excitation expected at about 650 cm^{-1} is overlapping with the strong electronic feature typical for all iridates [27], and the broad 750 cm^{-1}

FIG. 2. Temperature dependence of the Raman scattering spectra of $Pr_2Zr_2O_7$ in (a) (x, x) channel and (b) (x, y) channel.

FIG. 3. Temperature dependence of the Raman scattering spectra of Pr$_2$Ir$_2$O$_7$ in (x, x) channel.
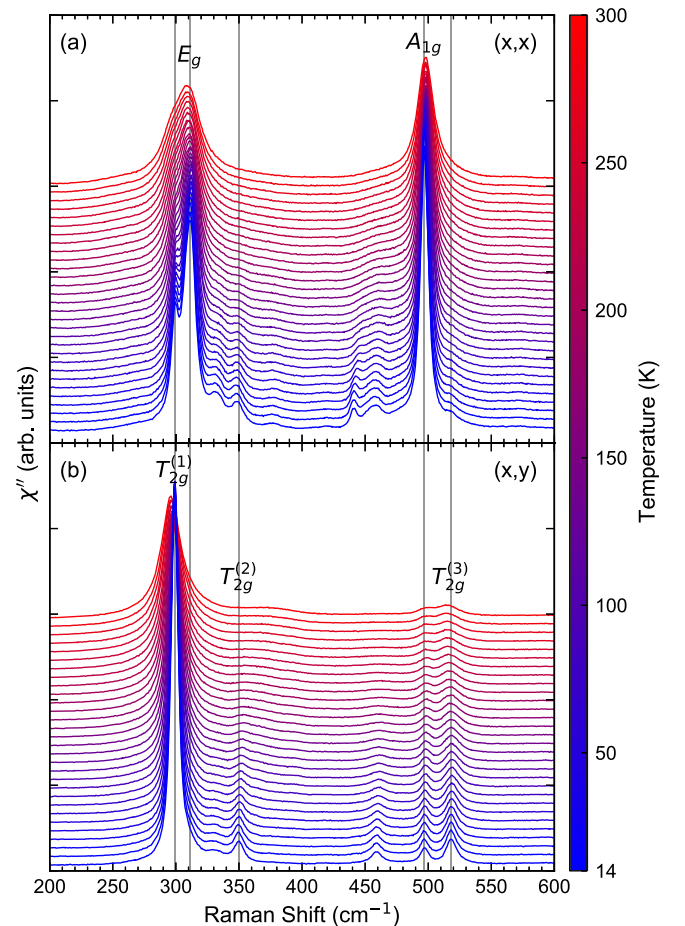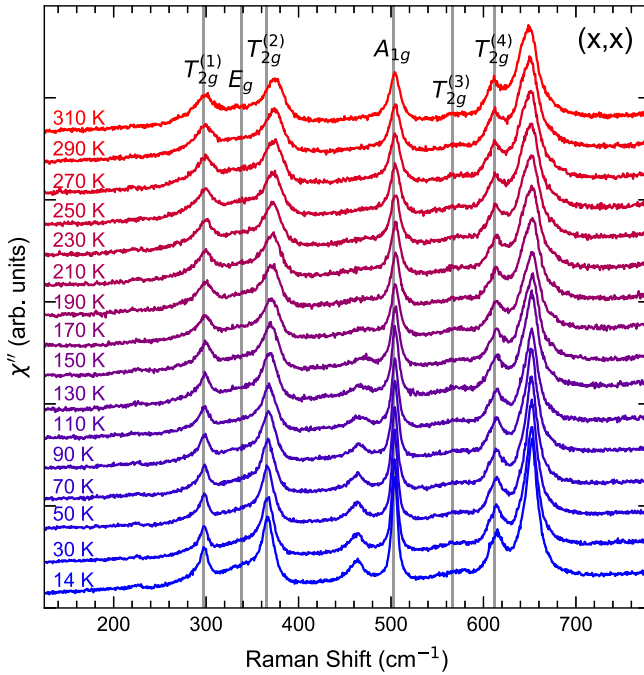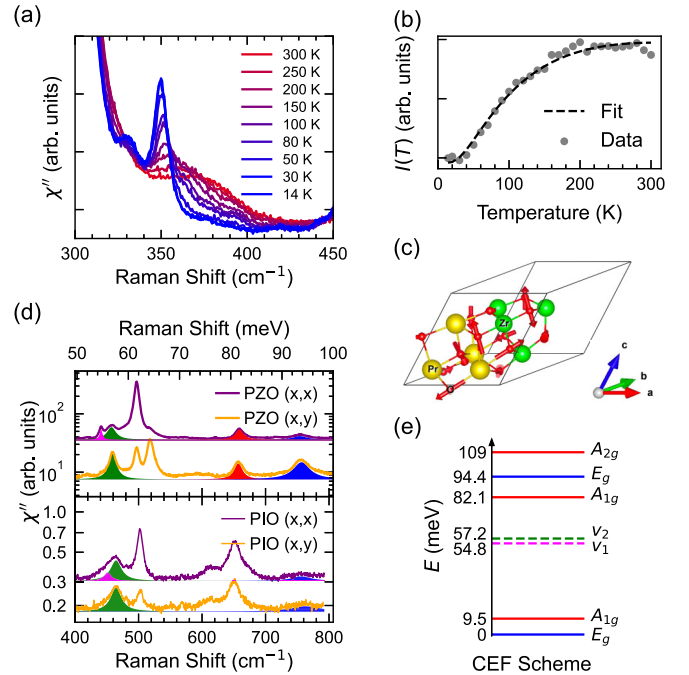

FIG. 4. (a) Temperature dependence of Raman scattering spectra of Pr$_2$Zr$_2$O$_7$ in the region of $A_{1g} \rightarrow E_g$ crystal electric field transitions in (x, y) channel. (b) Temperature dependence of spectral weight $I(T) = \int_{430\,\text{cm}^{-1}}^{330\,\text{cm}^{-1}} \chi''(\omega) d\omega$. (c) Atomic displacement of $T_{2g}^{(2)}$ phonon mode. (d) Raman spectra of Pr$_2$Zr$_2$O$_7$ (upper panel) and Pr$_2$Ir$_2$O$_7$ (lower panel) at 14 K in (x, x) and (x, y) channel on a log scale. Crystal field excitations are marked in different colors. Note the double feature of the excitation at about 450 cm^{-1} for both materials. (e) Crystal field scheme of Pr^{3+} ions in D_{3d} crystal environment. Energy values are provided for Pr$_2$Zr$_2$O$_7$.

excitation is observed only when using a 647 nm laser as an excitation line [see Fig. 4(c)]. While the energy of the CEF are similar to that of Pr$_2$Zr$_2$O$_7$ [23], they are considerably broadened (29 cm^{-1} in Pr$_2$Ir$_2$O$_7$ vs 12 cm^{-1} in Pr$_2$Zr$_2$O$_7$ at 14 K).

Additionally, in the spectra of Pr$_2$Ir$_2$O$_7$ we observe Raman scattering on interband electronic excitations at around 250 cm^{-1} (marked by yellow in Fig. 1) present in the spectra as a well-defined maximum due to a high density of states originating from the electronic bands in Pr$_2$Ir$_2$O$_7$ [28,29] and excitations typical for iridates at around 650 cm^{-1} (marked blue in Fig. 1) [27].

According to the symmetry analysis following the $Fd\bar{3}m$ symmetry of the unit cell, in the Raman spectra of Pr$_2$Zr$_2$O$_7$ and Pr$_2$Ir$_2$O$_7$ there are six Raman-active phonons (see Table II). Note that Pr and Zr (Ir) are Raman inactive. Experimentally observed frequencies of the phonons are in a good agreement with DFT calculations (see Table III). In the Raman spectra of both materials, A_{1g} and T_{2g} phonon bands appear as sharp peaks, while E_g phonons show more complicated spectra. The phonon lines of Pr$_2$Ir$_2$O$_7$ are broadened compared to Pr$_2$Zr$_2$O$_7$ spectra. For Pr$_2$Ir$_2$O$_7$, our experimental and calculated phonon spectra are in agreement with Ref. [30].

According to the calculations, E_g phonon frequency in Pr$_2$Zr$_2$O$_7$ spectra is expected at about 305 cm^{-1}. Instead, we observe two bands at 312 and 332 cm^{-1}, which are well resolved at low temperatures. Intensity of both bands follows polarization dependence of an E_g phonon in pyrochlores [30,31] (see also Fig. S1 in SM [11]), but the phonon band at 332 cm^{-1} shows a weaker polarization dependence (see Fig. S1 in SM [11]). The band of E_g vibration in Pr$_2$Ir$_2$O$_7$ spectra is found at about 334 cm^{-1}. It shows the largest width of all the Γ phonons of about 55 cm^{-1} and very weak

temperature dependence. While we cannot identify multiple components of this band as in Pr$_2$Zr$_2$O$_7$ spectra even at low temperatures, the large linewidth suggests an additional broadening or splitting into multiple partially overlapping components.

Figure 5 shows the temperature behavior of the widths and frequencies of the four lower frequency Raman-active phonons for Pr$_2$Zr$_2$O$_7$ (left panel) and Pr$_2$Ir$_2$O$_7$ (right panel) obtained by a fitting of the spectra by a sum of Lorentz line shapes. On a decrease of the sample temperature from 300 K, the phonons show hardening due to thermal contraction (see Fig. 2), except for $T_{2g}^{(2)}$ mode, which is discussed below. All phonons in Pr$_2$Zr$_2$O$_7$ show a conventional decrease of the linewidth due to phonon-phonon scattering [32], following the

TABLE II. Wyckoff positions and Γ point representations for Pr$_2$Zr$_2$O$_7$ (Pr$_2$Ir$_2$O$_7$).

Element	Wyckoff position	Γ representation
Pr	16c	Inactive
Zr (Ir)	16d	Inactive
O	48f	$A_{1g} + E_g + 3T_{2g}$
O$'$	8a	T_{2g}

TABLE III. Phonon modes assignment based on DFT calculation and experimental observation. Numbers inside the bracket denote the linewidth of the peak.

Mode	Frequency (cm^{-1})			
	$Pr_2Ir_2O_7$ DFT	$Pr_2Ir_2O_7$ Expt.	$Pr_2Zr_2O_7$ DFT	$Pr_2Zr_2O_7$ Expt.
$T_{2g}^{(1)}$	306	298 (13.0)	289	299 (6.7)
E_g	318	339 (40.8)	305	312 (9.8)
				332 (17.1)
$T_{2g}^{(2)}$	388	366 (14.4)	391	350 (9.7)
A_{1g}	487	503 (7.2)	466	499 (7.2)
$T_{2g}^{(3)}$	555	567 (27.7)	512	521 (9.4)
$T_{2g}^{(4)}$	633	615 (21.2)	719	

general formula

$$\Gamma_{ph\text{-}ph}(T) = \Gamma_0 + A[1 + 2n_B(\omega/2, T)]$$
$$+ B\{1 + 3n_B(\omega/3, T) + 3[n_B(\omega/3, T)]^2\}, \quad (1)$$

with Γ_0 of 5–7 cm^{-1}, depending on the phonon. The fitting parameters of $T_{2g}^{(1)}$, $T_{2g}^{(2)}$, and E_g modes in $Pr_2Zr_2O_7$ and

TABLE IV. Results of fitting for $Pr_2Zr_2O_7$ with the phonon-phonon scattering model.

Mode	Γ_0 (cm^{-1})	A (cm^{-1})	B (cm^{-1})
$T_{2g}^{(1)}$	1.901	4.811	0.188
E_g	4.239	6.861	0.048
A_{1g}	0	7.571	0.232

$Pr_2Ir_2O_7$ are presented in Tables IV and V. The subtle effects of phonon-electron scattering in $Pr_2Ir_2O_7$ become apparent when compared to the behavior of the $Pr_2Zr_2O_7$ phonons; see Fig. 5. At the lowest temperature, all of the $Pr_2Ir_2O_7$ phonons show larger width, while the temperature dependence of the width is less steep, and is described better by the scattering of phonons on interband transitions, as observed in semimetals [33],

$$\Gamma_{ph\text{-}el}(T) = \Gamma_0 + F[n_F(\hbar\omega_a, T) - n_F(\hbar\omega_a + \hbar\omega_{ph}, T)]. \quad (2)$$

The $T_{2g}^{(2)}$ phonon in the spectra of $Pr_2Zr_2O_7$ shows unconventional behavior different from that discussed above. In the spectral range of approximately 330–430 cm^{-1}, the changes of the spectra on cooling reveal the $T_{2g}^{(2)}$ phonon as a sharp band only below 100 K [see Fig. 4(a)]. The frequency of 380 cm^{-1} corresponds to a CEF transition from the first excited A_{1g} state at 77 cm^{-1} to the second excited state at about 440 cm^{-1} [see Fig. 4(e)]. In the first approximation, the total Raman intensity should be a superposition of CEF and phonon response, where CEF response will be changing as the population of the first excited A_{1g} level at $E_1 = 77$ cm^{-1} and the second excited at $E_2 = 440$ cm^{-1}. The spectral weight in this range can be calculated as $I(T) = \int_{330 \text{ cm}^{-1}}^{430 \text{ cm}^{-1}} \chi''(\omega)d\omega$ and is decreasing on cooling, indeed following a dependence of $I(T) = A + B(e^{-E_1/k_BT} - e^{-E_2/k_BT})$ [see Fig. 4(b)]. While the picture of a superposition of intensities works as a good approximation for the temperature dependence of the spectral weight, it does not explain the shape of the $T_{2g}^{(2)}$ phonon. In fact, the phonon appears as a weak antiresonance at the frequency of 371 cm^{-1} at room temperature and gains the shape of a peak as the spectral weight of the CEF decreases. The position of the $T_{2g}^{(2)}$ phonon defined as a position of an antiresonance or a maximum, depending on temperature, softens from 371 cm^{-1} down to 350 cm^{-1} on cooling from 300 K down to 14 K. The $A_{1g} \rightarrow E_g$ excitation is absent in $Pr_2Ir_2O_7$ spectra; however, the T_{2g} phonon shows moderate softening from the frequency from 375 cm^{-1} at room temperature down to 364 cm^{-1} at 14 K.
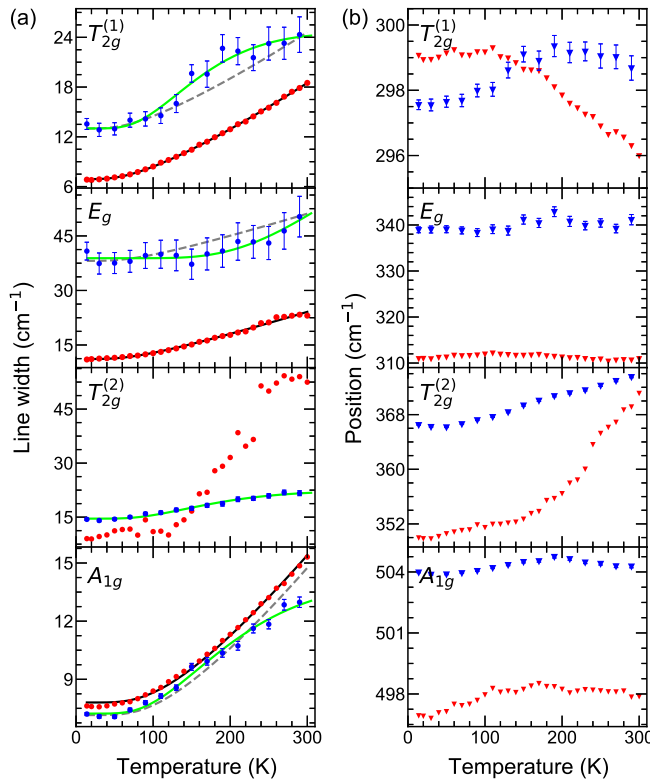

FIG. 5. Temperature dependence of (a) linewidths and (b) positions for $Pr_2Zr_2O_7$ (blue) and $Pr_2Ir_2O_7$ (red). Black lines are fits of linewidth of $Pr_2Zr_2O_7$ phonons with extended Klemens model. Dashed lines show the same temperature dependence with Γ_0 increased for $Pr_2Ir_2O_7$. Green lines are the fits of linewidth of $Pr_2Ir_2O_7$ phonons by the phonon-electron scattering model. Note that the temperature dependence for $Pr_2Ir_2O_7$ phonons is best fit by phonon-electron scattering.

TABLE V. Results of fitting for $Pr_2Ir_2O_7$ with the phonon-electron scattering model.

Mode	Γ_0 (cm^{-1})	F (cm^{-1})	ω_a (cm^{-1})
$T_{2g}^{(1)}$	13.017	66.444	243.654
E_g	38.430	619.369	775.777
$T_{2g}^{(2)}$	14.585	40.0453	256.860
A_{1g}	7.230	30.701	275.574

IV. DISCUSSION

A. Phonon-electron scattering

The energies of the phonon modes are very similar between Pr$_2$Ir$_2$O$_7$ and Pr$_2$Zr$_2$O$_7$, as expected for materials with similar crystal structures, which differ only by a substitution of B position in the $A_2B_2O_7$ of pyrochlore structure. However, the difference both in low-temperature width of the phonons and in their temperature dependence is considerable. At low temperatures, all the phonon bands of Pr$_2$Ir$_2$O$_7$ show larger linewidth than that of Pr$_2$Zr$_2$O$_7$. We assign this difference not to the larger random disorder in Pr$_2$Ir$_2$O$_7$, but to the effects of phonon-electron scattering. It was shown [33,34] that in semimetals, phonon can scatter on the direct ($q = 0$) interband transitions, producing a temperature dependence of width very different from one described by Klemens' model. This can explain the temperature behavior of the phonons in Pr$_2$Ir$_2$O$_7$ (Fig. 5). The fact that two phonons of different symmetries, T_{2g} and A_{1g}, which are not coupled to magnetic degrees of freedom, show the evidence of phonon-electron scattering suggests that the scattering occurs on the interband transitions away from the highest symmetry points of the BZ and is not restricted by symmetry. The high probability of such scattering could be explained based on the calculated Pr$_2$Ir$_2$O$_7$ band structure, which suggests a band touching at the Γ point of BZ and a narrow gap between nearly parallel bands between Γ and L points [29,35], while the calculations of Ref. [36] suggest these parallel bands below the Fermi energy. The gap in the range of 300–500 cm^{-1} (37–65 meV) between these bands would provide a suitable phase space for phonon-electron scattering on interband transitions. Moreover, the presence of this scattering testifies for the existence of such a band gap.

B. Crystal electric field excitations in Pr$_2$Ir$_2$O$_7$

The similar D_{3d} structural environment for Pr^{3+} in Pr$_2$Ir$_2$O$_7$ and Pr$_2$Zr$_2$O$_7$ results in similar CEF splitting, shown as a scheme in Fig. 4(e). The results of neutron scattering spectroscopy [25,37], our results on Raman scattering presented in this work and in Ref. [23], as well as the temperature dependence of magnetic susceptibility [24,26] support this assumption. High energy resolution of Raman scattering provides a possibility to quantify the broadening of the CEF by about 30 cm^{-1} in the semimetallic Pr$_2$Ir$_2$O$_7$ due to the interactions with the itinerant charge carriers compared to Pr$_2$Zr$_2$O$_7$ [38].

The excitation at 450 cm^{-1} (56 meV) in Pr$_2$Zr$_2$O$_7$ was shown to be vibronically coupled to a phonon, as evidenced by a strong polarization dependence of the split line of this excitation [23]. In the spectrum of Pr$_2$Ir$_2$O$_7$ the CEF are broadened, but a comparison of (x, x) and (x, y) polarization allows us to identify the polarization dependence and vibronic coupling in Pr$_2$Ir$_2$O$_7$ spectrum [see Fig. 4(d)]. The polarization dependence is weaker, which shows that the coupling is also weakened by the interactions with the charge carriers.

C. Changes of the structure on cooling

In addition to the vibronic coupling, typical for rare earth compounds [39] and discussed for the second excited E_g state

of Pr$_2$Zr$_2$O$_7$ [23], at temperatures above about 100 K we observe a coupling of the broadband of a transition between first and second excited CEF $A_{1g} \rightarrow E_g$ coupled to the $T_{2g}^{(2)}$ phonon found at about 350 cm^{-1}. Interestingly, this coupling does not result in the vibronic splitting which is not allowed by symmetry. Instead, at high temperatures we observe a broadband of the $A_{1g} \rightarrow E_g$ transition with a phonon feature present as an antiresonance, typical for Fano coupling [40]. As the intensity of the CEF transition decreases on cooling due to the depopulation of the A_{1g} level [Figs. 4(a) and 4(b)], the phonon appears in the spectra as a regular peak with a Lorentzian shape.

The same $T_{2g}^{(2)}$ phonon is the only one of the Raman active phonons in these two compounds showing softening on cooling (see Fig. 5). The eigenvector of this phonon involves a deformation of the Pr-O-Pr angle. This angle determines the size of the superexchange interactions between Pr atoms. Interestingly, such a change of the angle between Pr-O-Pr bonds on cooling was suggested to explain the temperature dependence of magnetic susceptibility in this material, linked to a decrease of superexchange J [26].

While the small scale of J in Pr$_2$Zr$_2$O$_7$ and the importance of crystal field levels for its magnetic properties makes it difficult to disentangle effects of the lattice on magnetic interactions, the subtle changes of the lattice on cooling can make magnetic parameters temperature dependent, with a change at around 100 K defined by the behavior of the lattice, and not the energy scale of magnetic parameters.

In the spectra of Pr$_2$Ir$_2$O$_7$, the softening of the $T_{2g}^{(2)}$ phonon is only 8 cm^{-1} compared to the 20 cm^{-1} observed for Pr$_2$Zr$_2$O$_7$, evidencing less temperature changes of the lattice. To our best knowledge, the temperature dependence of magnetic susceptibility in Pr$_2$Ir$_2$O$_7$ is in a good agreement with the crystal field model [7].

D. E_g phonons

Anomalous behavior was also detected from E_g phonons, which show a double band in the spectra of Pr$_2$Zr$_2$O$_7$, and an increased width in the spectra of Pr$_2$Ir$_2$O$_7$.

E_g degree of freedom is sensitive to magnetoelastic coupling in pyrochlore materials as revealed on magnetic phase transitions [30]. However, both compounds are known not to order magnetically, and the properties of the E_g phonons do not show any pronounced temperature dependence. A possible interpretation of a splitting of a doubly degenerate band observed in the whole temperature range is a local symmetry breaking. For the highest quality crystals of Pr$_2$Zr$_2$O$_7$ free from oxygen vacancies and site mixing [41], a shift of Pr ion from a central position [4,15], and a local tilting of octahedra [17], which reduces local symmetry from $Fd\bar{3}m$ (point group O_h) to $P4_32_12$ (point group D_4) is discussed. With this symmetry reduction, E_g phonons split into two in-plane modes of B_1 symmetry (see Table VI). T_{2g} phonons split into B_2 and E modes, where the E modes will be observed in xz and yz channels which can be only detected in out-of-plane scattering, and thus will not appear in the spectra in (x, y) and $(x^2 - y^2)$ channels. These symmetry considerations can explain why T_{2g} phonons do not show any anomalous behavior of their width.

TABLE VI. Correlations between O_h and D_4 groups and symmetries.

O_h		D_4	
A_{1g}	$(x^2+y^2+z^2)$	A_1 $(x^2+y^2,\ z^2)$	
E_g	$(x^2-y^2$ $2z^2-x^2-y^2)$	A_1+B_1 $\rightarrow$ B_1 (x^2-y^2)	
T_{2g}	(xy, xz, yz) $\longrightarrow$ $E+B_2$	B_2 (xy) E (xz, yz)	

The large width of E_g phonons in $Pr_2Ir_2O_7$ spectra, which appear to be about twice the width of the other phonons, suggest that a splitting of this band is also present in $Pr_2Ir_2O_7$, but cannot be resolved due to the large band width, and can have a similar origin.

V. CONCLUSIONS

In this work we compare the Raman phonon spectra of $Pr_2Zr_2O_7$ and $Pr_2Ir_2O_7$, which have a very similar crystal structure, but drastically different electronic properties. Raman phonons observed at similar frequencies demonstrate different behavior with temperature, determined by phonon-phonon scattering in the case of the insulating $Pr_2Zr_2O_7$ and phonon-electron scattering in the case of $Pr_2Ir_2O_7$. A softening of the phonon changing Pr-O-Pr angle on cooling explains the decrease of magnetic interactions J deduced previously from magnetic susceptibility measurements. The broadening of the E_g phonons demonstrates the presence of the disordered tilting of tetrahedra suggested for pyrochlore materials. As a whole, our study elucidates many subtle questions about electronic and magnetic properties of these materials through the behavior of the underlying lattice.

[1] J. S. Gardner, M. J. P. Gingras, and J. E. Greedan, Rev. Mod. Phys. **82**, 53 (2010).

[2] M. J. Gingras and P. A. McClarty, Rep. Prog. Phys. **77**, 056501 (2014).

[3] G. Chen, Phys. Rev. B **94**, 205107 (2016).

[4] S. Koohpayeh, J.-J. Wen, B. Trump, C. Broholm, and T. McQueen, J. Cryst. Growth **402**, 291 (2014).

[5] J. P. Clancy, H. Gretarsson, E. K. H. Lee, D. Tian, J. Kim, M. H. Upton, D. Casa, T. Gog, Z. Islam, B.-G. Jeon, K. H. Kim, S. Desgreniers, Y. B. Kim, S. J. Julian, and Y.-J. Kim, Phys. Rev. B **94**, 024408 (2016).

[6] J. Bertinshaw, Y. Kim, G. Khaliullin, and B. Kim, Annu. Rev. Condens. Matter Phys. **10**, 315 (2019).

[7] S. Nakatsuji, Y. Machida, Y. Maeno, T. Tayama, T. Sakakibara, J. van Duijn, L. Balicas, J. N. Millican, R. T. Macaluso, and J. Y. Chan, Phys. Rev. Lett. **96**, 087204 (2006).

[8] R. Flint and T. Senthil, Phys. Rev. B **87**, 125147 (2013).

[9] J. M. Ni, Y. Y. Huang, E. J. Cheng, Y. J. Yu, B. L. Pan, Q. Li, L. M. Xu, Z. M. Tian, and S. Y. Li, Nat. Commun. **12**, 307 (2021).

[10] X.-P. Yao and G. Chen, Phys. Rev. X **8**, 041039 (2018).

[11] See Supplemental Material at http://link.aps.org/supplemental/10.1103/PhysRevB.105.075137 for temperature dependence of linewidth and polarization dependence.

[12] K. Kimura, S. Nakatsuji, J. Wen, C. Broholm, M. Stone, E. Nishibori, and H. Sawa, Nat. Commun. **4**, 1934 (2013).

[13] D. E. MacLaughlin, O. O. Bernal, L. Shu, J. Ishikawa, Y. Matsumoto, J.-J. Wen, M. Mourigal, C. Stock, G. Ehlers, C. L. Broholm, Y. Machida, K. Kimura, S. Nakatsuji, Y. Shimura, and T. Sakakibara, Phys. Rev. B **92**, 054432 (2015).

[14] J. G. Rau and M. J. Gingras, Annu. Rev. Condens. Matter Phys. **10**, 357 (2019).

[15] N. Martin, P. Bonville, E. Lhotel, S. Guitteny, A. Wildes, C. Decorse, M. Ciomaga Hatnean, G. Balakrishnan, I. Mirebeau, and S. Petit, Phys. Rev. X **7**, 041028 (2017).

[16] N. Drichko, C. Broholm, K. Kimura, R. Ishii, and S. Nakasutji, Phys. Rev. B **93**, 184425 (2016).

[17] B. A. Trump, S. M. Koohpayeh, K. J. Livi, J.-J. Wen, K. Arpino, Q. M. Ramasse, R. Brydson, M. Feygenson, H. Takeda, M. Takigawa *et al.*, Nat. Commun. **9**, 2619 (2018).

[18] J. N. Millican, R. T. Macaluso, S. Nakatsuji, Y. Machida, Y. Maeno, and J. Y. Chan, Mater. Res. Bull. **42**, 928 (2007).

[19] G. Kresse and J. Furthmüller, Phys. Rev. B **54**, 11169 (1996).

[20] J. P. Perdew, K. Burke, and M. Ernzerhof, Phys. Rev. Lett. **77**, 3865 (1996).

[21] P. E. Blöchl, Phys. Rev. B **50**, 17953 (1994).

[22] G. Kresse and D. Joubert, Phys. Rev. B **59**, 1758 (1999).

[23] Y. Xu, H. Man, N. Tang, S. Baidya, H. Zhang, S. Nakatsuji, D. Vanderbilt, and N. Drichko, Phys. Rev. B **104**, 075125 (2021).

[24] Y. Machida, S. Nakatsuji, H. Tonomura, T. Tayama, T. Sakakibara, J. Van Duijn, C. Broholm, and Y. Maeno, J. Phys. Chem. Solids **66**, 1435 (2005).

[25] J.-J. Wen, S. M. Koohpayeh, K. A. Ross, B. A. Trump, T. M. McQueen, K. Kimura, S. Nakatsuji, Y. Qiu, D. M. Pajerowski, J. R. D. Copley, and C. L. Broholm, Phys. Rev. Lett. **118**, 107206 (2017).

[26] P. Bonville, S. Guitteny, A. Gukasov, I. Mirebeau, S. Petit, C. Decorse, M. C. Hatnean, and G. Balakrishnan, Phys. Rev. B **94**, 134428 (2016).

[27] T. Hasegawa, N. Ogita, K. Matsuhira, S. Takagi, M. Wakeshima, Y. Hinatsu, and M. Udagawa, J. Phys. Conf. Ser. **200**, 012054 (2010).

[28] G. Chen and M. Hermele, Phys. Rev. B **86**, 235129 (2012).

[29] F. Ishii, Y. P. Mizuta, T. Kato, T. Ozaki, H. Weng, and S. Onoda, J. Phys. Soc. Jpn. **84**, 073703 (2015).

[30] K. Ueda, R. Kaneko, A. Subedi, M. Minola, B. J. Kim, J. Fujioka, Y. Tokura, and B. Keimer, Phys. Rev. B **100**, 115157 (2019).

[31] M. Maczka, J. Hanuza, K. Hermanowicz, A. Fuentes, K. Matsuhira, and Z. Hiroi, J. Raman Spectrosc. **39**, 537 (2008).

[32] Y. Kim, X. Chen, Z. Wang, J. Shi, I. Miotkowski, Y. Chen, P. Sharma, A. Lima Sharma, M. Hekmaty, Z. Jiang *et al.*, Appl. Phys. Lett. **100**, 071907 (2012).

[33] G. B. Osterhoudt, Y. Wang, C. A. C. Garcia, V. M. Plisson, J. Gooth, C. Felser, P. Narang, and K. S. Burch, Phys. Rev. X **11**, 011017 (2021).

[34] J. Coulter, G. B. Osterhoudt, C. A. C. Garcia, Y. Wang, V. M. Plisson, B. Shen, N. Ni, K. S. Burch, and P. Narang, Phys. Rev. B **100**, 220301(R) (2019).

[35] T. Kondo, M. Nakayama, R. Chen, J. J. Ishikawa, E.-G. Moon, T. Yamamoto, Y. Ota, W. Malaeb, H. Kanai, Y. Nakashima, Y. Ishida, R. Yoshida, H. Yamamoto, M. Matsunami, S. Kimura, N. Inami, K. Ono, H. Kumigashira, S. Nakatsuji, L. Balents *et al.*, Nat. Commun. **6**, 10042 (2015).

[36] H. Zhang, K. Haule, and D. Vanderbilt, Phys. Rev. Lett. **118**, 026404 (2017).

[37] J. Van Duijn, K. Kim, N. Hur, R. Ruiz-Bustos, D. Adroja, F. Bridges, A. Daoud-Aladine, F. Fernandez-Alonso, J. Wen, V. Kearney *et al.*, Phys. Rev. B **96**, 094409 (2017).

[38] K. W. Becker, P. Fulde, and J. Keller, Z. Phys. B **28**, 9 (1977).

[39] P. Thalmeier, J. Appl. Phys. **55**, 1916 (1984).

[40] U. Fano, Phys. Rev. **124**, 1866 (1961).

[41] N. Tang, A. Sakai, K. Kimura, S. Nakamura, M. Fu, Y. Matsumoto, T. Sakakibara, and S. Nakatsuji, in *Proceedings of the International Conference on Strongly Correlated Electron Systems (SCES2019)* [J. Phys. Soc. Jpn. (2020)].